Hindawi
International Journal of Photoenergy
Volume 2022, Article ID 4528768, 8 pages
https://doi.org/10.1155/2022/4528768

Research Article

Effects of Different Particle-Sized Al Powders on Sintering Properties of Aluminum Paste in Crystalline Silicon Solar Cell

Peng Zhu, Yang Lu, and Xiaolei Chen

College of Chemistry and Chemical Engineering, Nantong University, Nantong 226019, China

Correspondence should be addressed to Xiaolei Chen; cxl800405@126.com

Received 5 July 2022; Revised 19 September 2022; Accepted 7 October 2022; Published 3 November 2022

Academic Editor: Weijie Yang

In this paper, the effects of particle size difference of aluminum (Al) powder on physical properties of Al powder and sintering properties of Al paste were investigated. For this purpose, respectively, Al powders with four mean particle sizes were used, which were obtained by two classifications using the same nitrogen atomization process. Thermal analysis results showed that the smaller the Al particle size, the lower the oxidation temperature and the higher the reaction enthalpy, indicating higher reactivity of the Al powder. Four Al powders were prepared into Al paste by the same process, and the resistances of the paste increased with the decrease of the particle size of the aluminum powder. Electrochemical capacitance-voltage profiler (ECV) and scanning electron microscope (SEM) analysis showed that the smaller the Al particle size, the thicker the back surface field (BSF) and the higher the doping concentration of BSF. It was found that the smaller size of Al powder limited the migration of silicon, which resulted in higher concentration of silicon (Si) in the Al-Si liquid phase. This leads to reaching a balance at a higher temperature between the recrystallization of silicon from the alloy liquid and the dissolution of silicon in the liquid alloy and a higher doping concentration and a higher effective BSF doping thickness. Results of the study will provide reference for further study and application of Al paste.

1. Introduction

In crystalline silicon solar cell aluminum (Al) paste, Al powder is more than 70 wt% and has the decisive influence to the performance of the Al paste. The contact resistance of Al paste between the p+ electrodes strongly was decreased for higher Al content in the paste [1]. The particle size of Al powder also strongly affects the electrical characteristics of Al paste. An investigation on the effects of particle size of Al powder in silver/Al paste on n-type solar cells showed that the contact resistance decreases with increasing the particle size of the powder. In addition, the optimization of the particle size of Al powder can effectively increase efficiency of the cells [2]. Another study showed that only larger Al particles can be totally filled with silicon (Si), and this is explained by the lower internal pressure of the larger particles compared with the smaller ones [3]. Many experiments showed that applied Al nanoparticles enhance the performance of crystalline solar cell [4–6]. Rassekh et al. [7] showed how different shapes of Al nanoparticles affect absorption enhancement in silicon thin-film solar cells.

Figure 1 is a typical scanning electron microscope (SEM) diagram of back surface field (BSF) formed by Al paste sintering. It could be seen from Figure 1 that the Al powder did not melt completely in the sintering process, and an obvious Al doped P^+ layer was formed.

As we all know, when the sintering temperature increases to 300°C, silicon at the Al-Si interface starts to dissolve into Al; when the sintering temperature reaches the eutectic temperature (577°C), Al-Si alloy liquid phase is generated at the Al-Si interface [8]. As the temperature further rises, the Al-Si alloy liquid phase and the proportion of silicon element in the liquid phase both increase. In the process of forming Al-Si liquid phase, Si and Al thermal are diffused into each other, Si migrated rapidly in the Al layer, and Al is doped in the Si matrix [9, 10]. In the process of cooling, the thermal diffusion of Al and the recrystallization of Si jointly formed a heavily doped P^+ layer. When the temperature is

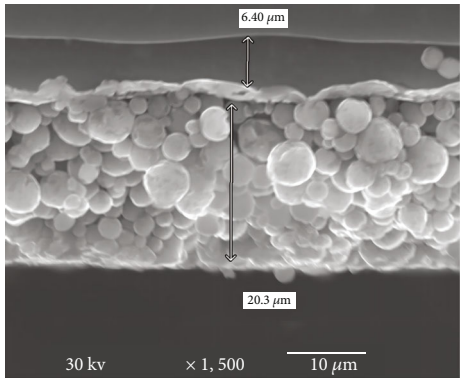

Figure 1: SEM image of BSF formed by Al paste sintering.

below 577°C, Al-Si liquid phase is cured to form Al-Si alloy layers [11, 12].

In the sintering and cooling process, the Al powder has an oxide film on its surface, which is further oxidized and thickened with the temperature increasing. So even if the temperature rises above 660°C, the Al powder will not be melted completely. In the study conducted by Liu et al. [13], the effects of melted glass and temperature on the aluminum oxide film were studied. Their results showed the oxide film of the aluminum powder effected conductive contact points (surfaces) which are formed at the interface between the aluminum powder particles. Zanesco et al. [14] presented the influence of Al paste surface density on the electrical parameters of silicon solar cells; however, the related effects of Al powder are not mentioned.

The formation mechanism of Al-Si contact [15–19] and the influence of Al BSF on cell performance have been thoroughly studied [20–22]. However, relevant researches were mostly focused on the changes in cell performance caused by paste [23–25]. Each of these phenomena needs to be investigated, particularly how each may be impacted by the parameters of the Al powder.

A review of the literatures shows that no systematic study has been conducted about the particle size of Al powder on sintering properties of Al paste. Therefore, in this study, the effects of the Al powder particle size on physical properties of Al powder, the resistivity and microstructure of Al paste, and the Al-Si contact during Al paste sintering will be investigated. For this purpose, four Al powders of different particle sizes were chosen and the four Al paste samples were prepared with the same formula as research samples.

2. Experimental

2.1. Al Powder. The Al powder used was provided by Hunan Goldsky Aluminum Industry High-Tech Co., Ltd., and the series Al powders were prepared by nitrogen atomization. The general process of nitrogen atomization includes Al ingot melting, powder atomization, and Al powder classification and packing, which are all done under nitrogen protection. Here, four Al powder samples with particle sizes from small to large were identified as PS3, PS5, PS7, and PS9 were selected (the physical properties of four Al powder samples are listed in Table 1).

2.2. Paste Preparation. The four Al paste samples were identified as PSP3, PSP5, PSP7, and PSP9 and prepared with the same formula. The formula composition is shown in Table 2. The same kinds of glass frit, additive, and organic vehicle (solution of ethyl cellulose in solvent) were mixed with different Al powders and the ratio of Al powder/vehicle/frit/additive was 76.05/22.0/1.5/0.45. The pastes were prepared and homogenized on a standard stirring and a three roll mill (EXAKT 80E).

2.3. Printing and Sintering. The four Al pastes were screen printed through a stainless steel stencil (mesh no. 280, wire diameter 23 μm, thickness 45 μm, and tension 28 N) on an alumina substrate and a mono-Si wafer using a printer (AT-60PD, Dongyuan Machinery Manufacturing Co., Ltd.). The printing was carried out at the optimized snap-off between stencil and substrate; then pressure and speed were applied to the roller on the stencil in order to obtain a wet film roughly 30 μm thick. These wet films were dried at 200°C in an infrared drying oven for 1 min and then sintered in BTU 609 infrared tunnel furnace. The sintering curve is shown in Figure 2.

2.4. Property Characterization. The particle size and particle size distribution of the four Al powders were tested by laser particle size instrument (Malvin Company, Model Company 2000). The oxygen content of Al powder was tested by oxygen nitrogen hydrogen analyzer (Steel Yanak 3000). The specific surface area of Al powder was tested by BET measurements (Biaoda Company, Model SSA-4000). The thermal behavior of Al powder was analyzed by a synchronous thermal analyzer (STA) (NETZSCH Company, Model STA449F3). A four-probe square resistance tester (Suzhou Lattice Company, Model ST2253-F01) was used to measure the square resistance of Al layer. A scanning electron microscope and an energy disperse spectrometer (Zeiss Gemini Company, Model SEM300) were used to observe the morphology of Al film, thickness of BSF layer, and element composition of Al film. The doping concentration and depth of the Al paste were measured by electrochemical capacitance-voltage profiler (ECV) (WEP Company, Model CVP21).

3. Results and Discussion

3.1. Effect of Particle Size Difference on Properties of Al Powder. Al is a highly reactive amphoteric metal with an oxide layer on the surface. In the process of atomizing Al powder, the thickness and compactness of the oxide layer on the surface of Al powder were adjusted by the volume percentage of oxygen in nitrogen and the insulation temperature of Al liquid. PS3, PS5, PS7, and PS9 were series Al powders with different particle sizes obtained by the same nitrogen atomization process (the volume percentage of oxygen in nitrogen was 0.35%, and the insulation temperature of liquid Al was 885°C). The results of series Al powder

Table 1: Particle size, specific surface area, and oxygen content of different aluminum powder.

	Particle size				Specific surface area (m^2/kg)	Oxygen content (%)
	D10 (μm)	D50 (μm)	D90 (μm)	Span		
PS3	1.83	3.95	6.88	1.079	682	0.523
PS5	3.35	5.02	7.41	0.808	475	0.431
PS7	5.08	8.07	12.54	0.925	301	0.371
PS9	6.62	10.10	15.06	0.835	238	0.327

Table 2: Aluminum paste composition.

Samples	Aluminum powder				Glass frit	Ethyl cellulose	Solvent	Additive
	PS3	PS5	PS7	PS9				
PSP3	76.05				1.5	2.0	20.0	0.45
PSP5		76.05			1.5	2.0	20.0	0.45
PSP7			76.05		1.5	2.0	20.0	0.45
PSP9				76.05	1.5	2.0	20.0	0.45

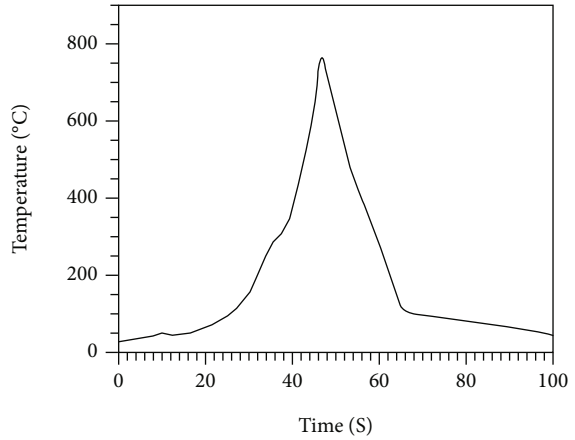

Figure 2: Sintering curve of sintering furnace.

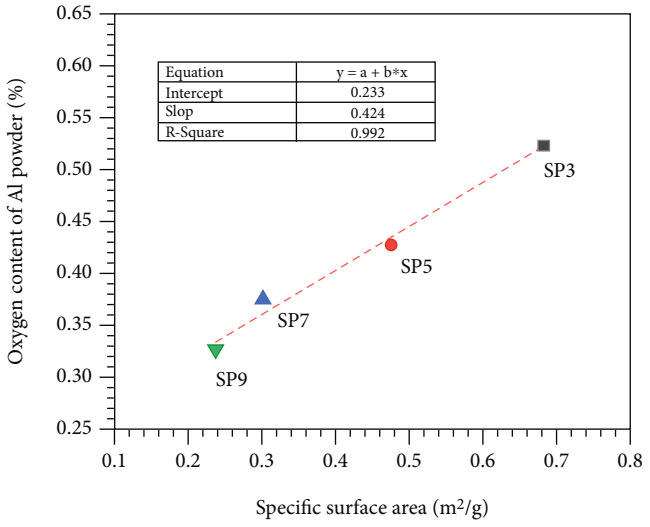

Figure 3: Relation between oxygen content and specific surface area of Al powder with different particle sizes.

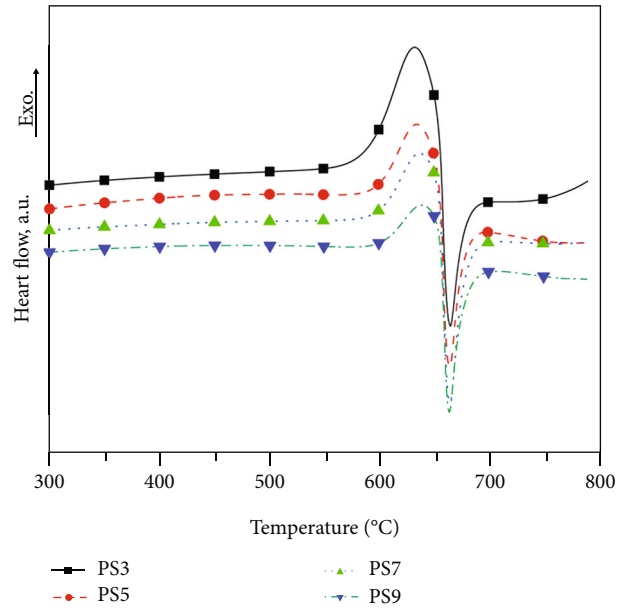

Figure 4: The DSC curve of different Al powder.

particle size, specific surface area, and oxygen content are shown in Table 1.

Generally, the smaller the particle size of the powder, the larger the specific surface area, and the greater the surface energy, the greater the physical and chemical reactivity. Therefore, for the four Al powders, we often believed that the oxide layer formed on the surface of Al powder was thicker than that of the larger Al powder. The results in Table 1 shows that both the specific surface area and oxygen content of the four Al powders decreased with the increasing particle size. Further, the relationship between the oxygen content and the surface area of the Al powder is shown in Figure 3. The R value of linear fitting was 0.99 calculated from Figure 3, which shows a good linear correlation. The results indicated that the thickness of oxide layer with

Table 3: DSC temperature parameters of different aluminum powder.

	The initial exothermic temperature (°C)	The exothermic peak temperature (°C)	Exothermic enthalpy ($J \cdot g^{-1}$)	The endothermic peak temperature (°C)
PS3	587.9	632.2	376.2	664.5
PS5	596.2	633.9	255.8	663.9
PS7	599.9	636.7	172.5	664.1
PS9	604.4	638.6	123.7	663.6

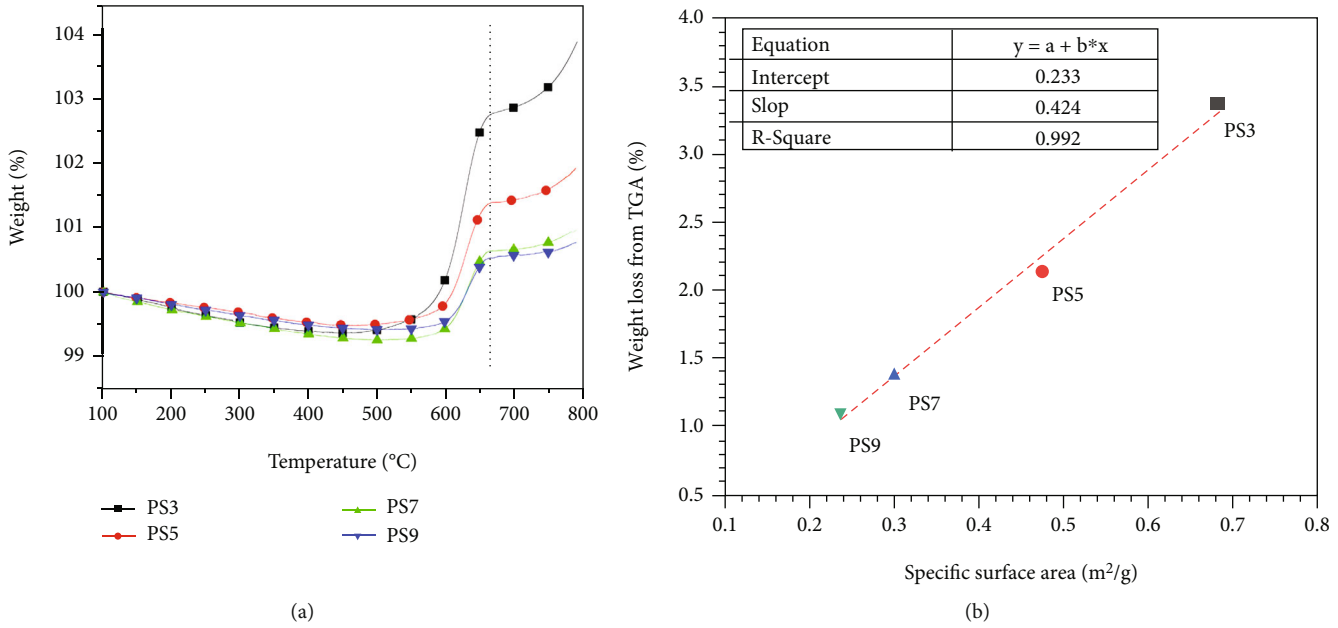

Figure 5: (a) TG curve of four Al powders and (b) relation diagram of thermal weight gain and specific surface area of Al powders.

Table 4: The resistivity of four aluminum pastes printed on different substrates.

	PSP3	PSP5	PSP7	PSP9
Alumina substrate	1.70×10^{-5}	1.52×10^{-5}	1.21×10^{-5}	1.04×10^{-5}
Monocrystalline silicon	2.21×10^{-5}	2.04×10^{-5}	1.75×10^{-5}	1.66×10^{-5}

different Al powder particle sizes was basically the same in the same nitrogen atomization process.

In practice, Al paste was sintered in air atmosphere, so we used the method of thermal analysis to study the performance change of Al powder heated in air atmosphere. Figure 4 shows the DSC curves of the four Al powders (the test condition was air atmosphere, heating rate of 20°C/min). It can be seen from Figure 4 that Al powder of each particle size had an exothermic peak and an endothermic peak, and the corresponding peak temperature parameters are listed in Table 3. Obviously, the exothermic process in DSC corresponded to the oxidation process of Al powder. Combined with the characteristic temperature in Table 3, the initial temperature and peak temperature of the exothermic peak both increased with the increasing particle size of Al powder; that is, the smaller the particle size of Al powder, the lower the temperature of oxidation reaction. The initial oxidation temperature and peak temperature of Al powder were defined as the sintering activity temperature of Al powder. Combined with the characteristic that the exothermal enthalpy increased with decreasing Al powder particle size, it could be confirmed that the sintering activity of Al powder was increased with decreasing Al powder particle size. We believed that this sintering activity was mainly related to the specific surface area of Al powder. The larger the specific surface area of Al powder, the larger the heat conduction area per unit weight, and the shorter the time required for heat equilibrium under the same heating conditions, the lower the oxidation reaction temperature of Al powder.

As can be seen from Table 3, the endothermic peak shapes of the four Al powders were basically the same, the peak temperature of each Al powder was around 664°C. The endothermic process was corresponded to Al powder melting.

Figure 5(a) shows the TGA (thermogravimetric analysis) curve of the four Al powders. The test atmosphere was air, and the heating rate was 20°C/min. As can be seen from the Figure 5(a), the four Al powders showed slight weight

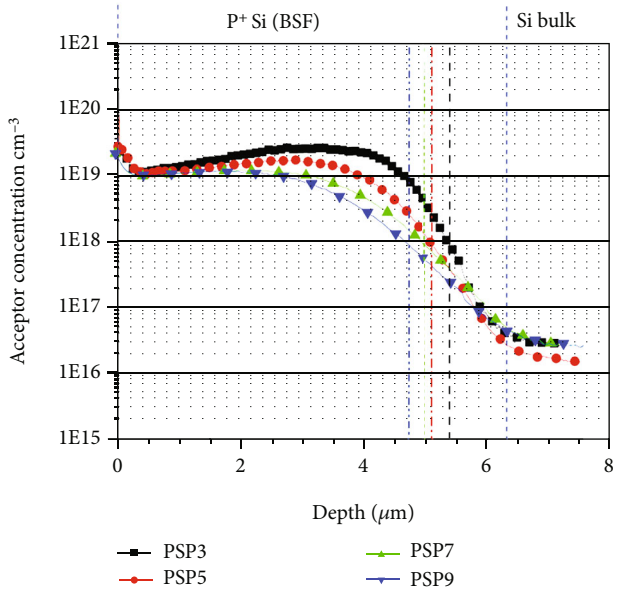

Figure 6: ECV curve of four kinds of Al paste.

loss at the initial stage and weight increase after reaching a certain temperature. The slight weight loss could be attributed to the certain moisture absorption on the surface of the Al powder, which was gradually volatilized during heating. After heating to a certain temperature, the weight increases could be attributed to the oxidation of the surface of the aluminum powder, which was consistent with the DSC exothermic process.

The weight gain ratios of each Al powder from the temperature of maximum loss point to 664°C on the TGA curve were calculated, which corresponded to the oxidation of Al powder during heating. The specific surface areas were plotted according to the weight increase ratios of the four Al powders, as shown in Figure 5(b). The R value of linear fitting was 0.992 calculated from Figure 5(b), which showed that the oxidation ratios of four Al powders during heating were all linearly correlated with their specific surface areas. The results showed that the surface of Al powders with different particle sizes in the same atomization process would be further oxidized during heating in air, and the increases of oxide layer thickness were not affected by the particle size.

3.2. Effect of Particle Size of Al Powder on Sintering Property of Al Paste. The Al pastes prepared by the four Al powders were printed on alumina ceramic substrate and mono-Si wafer, respectively. After drying and sintering the four pastes, the square resistance and the Al film thickness were measured; then the resistivity was calculated and is listed in Table 4.

Two trends could been seen in Table 4:

(1) The resistivity of the Al paste on alumina substrate was less than that on mono-Si wafer, respectively. On the alumina ceramic substrate, during the sintering process, when the temperature was risen above the melting temperature of Al, the liquid Al appeared in Al particles. Then, under the action of glass powder corrosion and internal pressure, the liquid Al broke through the surface oxide layers to achieve the mutual bonding between Al powder particles, while, as discussed above, on the mono-Si wafer substrate, during the sintering process, when the temperature was risen above 300°C, the silicon was dissolved in the Al powder. Then, when the temperature was risen above 577°C, Al-silicon eutectic was formed on the interface. Finally, as the temperature was risen further above the melting temperature of Al, the liquid Al broke through the surface oxide layer. Thus, on the mono-Si wafer substrate, the Al particles were bonded to each other by Al-silicon alloy liquid phase, and the resistivity of Al was increased with increasing silicon content.

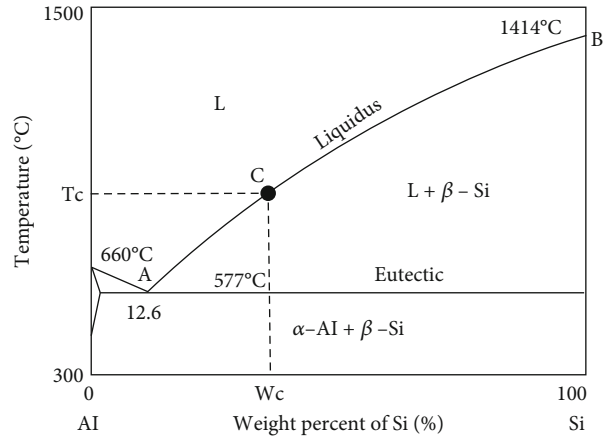

Figure 7: Al-Si phase diagram.

(2) On both the alumina ceramic substrate and mono-Si wafer, the resistivity of the pastes was decreased with increasing the size of Al powder. Balucani et al. [3] believed that this phenomenon was mainly caused by the fact that Al powder with larger particle size could absorb more silicon and the difference in the curvature radius of Al powders. However, according to the sintering characteristics of Al powder, because the Al powder with smaller particle size began to be oxidize at a lower temperature, it was believed that in the rapid sintering process, the further oxidation degree of the Al powder with small particle size was greater than that with large particle size, so the resistivity of the corresponding Al paste was greater. In order to verify the effect of oxygen content on the resistivity, we divided the same Al powder into two parts, one part was directly made into Al paste, and the other part was made into Al paste after increasing oxygen content by thermal oxidation. The experimental results showed that the resistivity of Al paste was increased significantly with the increasing the oxygen content.

Diluted hydrochloric acid was used to remove and clean the Al layer on the mono-Si wafer for an ECV test. The ECV curves of the four Al pastes are shown in Figure 6. It could

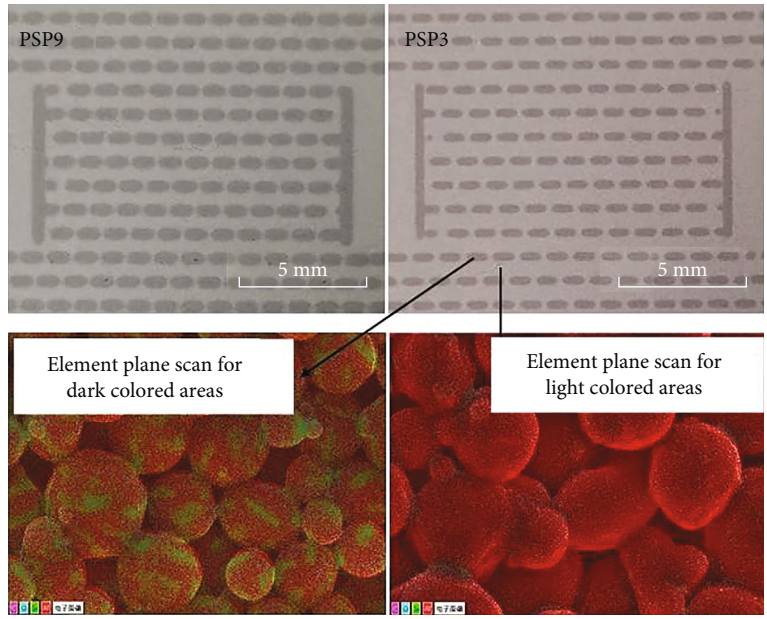

Figure 8: Sintering appearance and element distribution of the Al paste.

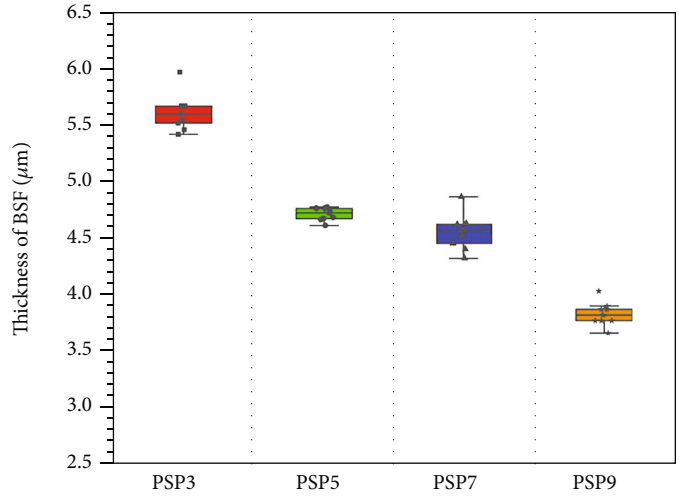

Figure 9: The BSF thickness of different Al paste.

be seen that the four Al pastes were effectively doped with silicon, and the bulk doping concentration of mono-Si wafer was 3×10^{16} cm^{-3}; the doping depth of the four Al paste had little difference. However, the highest doping concentrations of the Al pastes were decreasing with increasing Al particle size, indicating that the smaller Al particles contributed to the increase of BSF doping concentration. According to Kwang Su Choe's simulation, when the BSF doping concentration was lower than 1×10^{18} cm^{-3}, the cell efficiency increased with the increase of doping concentration. When the BSF doping concentration reached 1×10^{18} cm^{-3} and above, the cell efficiency was mainly affected by the thickness of BSF, and the thicker BSF, the higher the cell efficiency [26]. Therefore, if the effective BSF thickness is defined as the thickness with the doping concentration of 1×10^{18} c m^{-3} and above, it could be seen from the Figure 6 that the effective BSF thickness of the Al paste became thinner with the increase of the Al particle size.

It is known that BSF is formed by thermal diffusion of Al and recrystallization of silicon from Al-Si alloy liquid [27, 28]. In the process of appearing Al-Si alloy liquid phase to the highest temperature, BSF was mainly formed by thermal diffusion of Al, and the recrystallization rate was less than the dissolution rate and migration rate of silicon from wafer. When it reached the maximum temperature and began to cool, both the thermal diffusion rate and the doping concentration of Al reached the maximum and began to decrease, and the proportion of silicon in the liquid Al-Si alloy reached the maximum.

If the maximum doping concentration in BSF was determined by the thermal diffusion process of Al, then, the maximum doping concentration of BSF formed by the four Al

pastes under the same sintering process should be about the same; however, this is not the case at all. The results showed that the maximum doping concentration of BSF was determined by the recrystallization process of silicon. Therefore, we believed that in the Al paste sintering process, when the recrystallization rate of silicon exceeded the dissolution and migration rate of silicon, the concentration of BSF reached the highest. However, this point was not the highest temperature, but when it cooled to a certain temperature, the proportion of silicon in the liquid phase of Al-Si alloy reached the equilibrium point of solid-liquid phase separation line in the Al-Si phase diagram, as shown in Figure 7. Figure 7 shows the Al-Si phase diagram. AB was the solid-liquid phase separation line. Take point C on the AB line as an example; the proportion of silicon in the Al-silicon alloy liquid phase was defined as W_c. When the temperature fell below T_c, Si was recrystallized from the alloy liquid. Therefore, the temperature of recrystallization was dependent on the concentration of Si in the Al-Si liquid alloy.

Above all, the characteristics of Al paste sintering to form BSF in this study were as follows: (1) the total thickness of BSF was determined by the thermal diffusion of Al, and the effective thickness and highest doping concentration of BSF were determined by the recrystallization temperature of silicon; (2) the smaller size of Al powder limited the migration of silicon, which resulted in higher concentration of silicon in the Al-Si liquid phase, which led to reaching a balance at a higher temperature between the recrystallization of silicon from the alloy liquid and the dissolution of silicon in the liquid alloy and having higher doping concentration and higher effective BSF doping thickness.

In order to further verify our views, we printed the four Al pastes on the mono-Si wafer, respectively, whose surfaces were passivated by alumina and SiN_x film and opened by laser. The appearance pictures after drying and sintering are shown in Figure 8. The comparison of PSP3 with the smallest particle size and PSP9 with the largest particle size is shown in Figure 8.

Figure 8 shows that the laser opening area on the surface of the Al layer was darker, while the nonlaser opening area was lighter. SEM and energy spectrum were used to carry out element surface scanning analysis on the dark color area and light color area, respectively. A large amount of silicon was found in the dark color area, while very little silicon was found in the light color area. The contrast between PSP3 and PSP9 in Figure 8 showed that silicon was entered into Al particles and migrated rapidly in the sintering process, but the migration distance was affected by the particle size of Al powder. The larger the particle size of Al powder, the farther the migration distance of silicon.

In addition, we used SEM to measure the thickness of BSF formed by the sintering of four Al pastes at the laser opening, as shown in Figure 9. It was observed from Figure 9 that the thickness of BSF was increased with the decrease of Al particle size. These experimental results were in good agreement with our understanding of BSF formed by Al paste sintering, which will help to guide the development of Al paste for various crystalline silicon solar cells.

4. Conclusions

Al powder plays a decisive role in the performance of Al paste in crystalline silicon solar cell Al paste. Therefore, the Al powder particle size and the physical properties could have a great influences on the resistivity and microstructure of Al paste and the Al-Si contact during Al paste sintering. For this purpose, four Al powders of different particle sizes were chosen and the four Al paste samples were prepared with the same formula as research samples.

The results can be summarized as follows.

The oxygen content and specific surface area of these Al powders were both increased with the decrease of particle sizes, and the surface oxide layer thickness of four Al powders with different particle sizes was basically the same. Al particle size mainly affected the thermal oxidation reaction temperature and reaction speed, and the degree of oxidation reaction was only related to specific surface area.

The resistivity of the series of Al paste was decreased with the increase of the size of the Al powder. Due to the involvement of silicon in the sintering process of Al paste, the resistivity of Al paste on the mono-Si wafer was greater than that on the alumina substrate.

The smaller the particle size of Al powder, the thicker the effective BSF, and the higher the doping concentration of BSF. These are attributed to the smaller size of Al powder limited the migration of silicon, which resulted in higher concentration of silicon in the Al-Si liquid phase.

Data Availability

The data used to support the findings of this study are included within the article and are available from the corresponding author upon request.

Conflicts of Interest

The authors declare that they have no conflict of interest.

Acknowledgments

This work was supported by Nantong Science and Technology Bureau (Project No. JC2019090).

References

[1] H. Kerp, S. Kim, R. Lago et al., "Development of screenprintable contacts for p+ emitters in bifacial solar cells," in *21st European Photovoltaic Solar Energy Conference*, pp. 1–3, Dresden, Germany, 2006.

[2] T. Aoyama, M. Aoki, I. Sumita et al., "Effects of particle size of aluminum powder in silver/aluminum paste on n-type solar cells," *AIMS Materials Science*, vol. 5, no. 4, pp. 614–623, 2018.

[3] M. Balucani, L. Serenelli, K. Kholostov et al., "Aluminum-silicon interdiffusion in screen printed metal contacts for silicon based solar cells applications," *Energy Procedia*, vol. 43, pp. 100–110, 2013.

[4] Z. Q. Zhou, L. X. Wang, W. Shi, S. L. Sun, and M. Lu, "A synergetic application of surface plasmon and field effect to

improve Si solar cell performance," *Nanotechnology*, vol. 27, no. 14, article 145203, 2016.

[5] V. Kochergin, L. Neely, C.-Y. Jao, and H. D. Robinson, "Aluminum plasmonic nanostructures for improved absorption in organic photovoltaic devices," *Applied Physics Letters*, vol. 98, no. 13, article 133305, 2011.

[6] F. Hu, Z. Q. Zhou, L. Ma, C. Zhang, W. J. Zhou, and M. Lu, "Enhancing the ultraviolet-visible-near infrared photovoltaic responses of crystalline-silicon solar cell by using aluminum nanoparticles," *Physica E: Low-dimensional Systems and Nanostructures*, vol. 94, pp. 174–177, 2017.

[7] M. Rassekh, R. Shirmohammadi, R. Ghasempour, F. R. Astaraei, and S. F. Shayesteh, "Effect of plasmonic aluminum nanoparticles shapes on optical absorption enhancement in silicon thin-film solar cells," *Physics Letter A*, vol. 408, article 127509, 2021.

[8] X. J. Sun, J. J. Xing, Y. X. Yang, X. Yuan, H. B. Li, and H. Tong, "Ohimc contact formation mechanism of silver–aluminum paste metallization on the p+ emitter of n-type crystalline silicon solar cells," *Journal of Electronic Materials*, vol. 51, no. 10, pp. 5717–5722, 2022.

[9] M. Rauer, M. Rüdiger, C. Schmiga et al., "Incomplete ionization of aluminum in silicon and its effect on accurate determination of doping profiles," *Journal of Applied Physics*, vol. 114, no. 20, article 203702, 2013.

[10] W. H. Chen, R. Z. Liu, Q. G. Zeng, and L. Zhou, "Low cost multicrystalline bifacial PERC solar cells - fabrication and thermal improvement," *Solar Energy*, vol. 184, pp. 508–514, 2019.

[11] S. Siraj, S. Tahir, A. Ali, N. Amin, K. Mahmood, and A. Manzoor, "Assessing the impact of front grid metallization pattern on the performance of BSF silicon solar cells," *Silicon*, vol. 13, no. 12, pp. 4237–4245, 2021.

[12] G. P. Du, B. Chen, N. Chen, and R. Y. Hu, "Efficient boron doping in the back surface field of crystalline silicon solar cells via alloyed-aluminum-boron paste," *IEEE Electron Device Letters*, vol. 33, no. 4, pp. 573–575, 2012.

[13] S. K. Liu, X. Y. Zhu, and J. M. Long, "Sintering mechanism of electronic aluminum paste and its effect on electrical conductivity of aluminum electrode," *Material Science in Semiconductor Processing*, vol. 139, article 106352, 2022.

[14] I. Zanesco, V. A. Gonçalves, and A. Moehlecke, "Influence of the aluminum paste surface density on the electrical parameters of silicon solar cells," *Energy Procedia*, vol. 57, pp. 47–55, 2014.

[15] L. Sardi, S. Bargioni, C. Canali, M. Prudenziati, and V. Valbusa, "Some features of thick film technology for the back metallization of solar cells," *Solar Cells*, vol. 11, no. 1, pp. 51–67, 1984.

[16] G. Schubert, F. Huster, and P. Fath, "Physical understanding of printed thick-film front contacts of crystalline Si solar cells–review of existing models and recent developments," *Solar Energy Material and Solar Cells*, vol. 90, no. 18-19, pp. 3399–3406, 2006.

[17] K. C. Chuang and W. H. Lee, "Improvement on conductivity for thick film aluminum paste," *Journal of Nanoscience and Nanotechnology*, vol. 21, pp. 4715–4725, 2021.

[18] S. Riegel, F. Mutter, T. Lauermann, B. Terheiden, and G. Hahn, "Review on screen printed metallization on p-type silicon," *Energy Procedia*, vol. 21, pp. 14–23, 2012.

[19] Y. Lv, Y. F. Zhuang, W. J. Wang et al., "Towards high-efficiency industrial p-type mono-like Si PERC solar cells," *Solar Energy Materials and Solar Cells*, vol. 204, article 110202, 2020.

[20] M. Rauer, C. Schmiga, M. Glatthaar, and S. W. Glunz, "Quantitative theoretical and experimental analysis of alloying from screen- printed aluminum pastes on silicon surfaces," *Solar Energy Material and Solar Cell*, vol. 176, pp. 295–301, 2018.

[21] E. Urrejola, K. Peter, H. Plagwitz, and G. Schubert, "Distribution of silicon in the aluminum matrix for rear passivated solar cells," *Energy Procedia*, vol. 8, pp. 331–336, 2011.

[22] E. Urrejola, K. Peter, H. Plagwitz, and G. Schubert, "Silicon diffusion in aluminum for rear passivated solar cells," *Applied Phyics Letters*, vol. 98, no. 15, article 153508, 2011.

[23] S. Park, S. Bae, H. Kim et al., "Effects of controllable process factors on Al rear surface bumps in Si solar cells," *Current Applied Physics*, vol. 12, no. 1, pp. 17–22, 2012.

[24] K. Dressler, M. Kratt, P. A. Voss, S. Ebert, A. Herguth, and G. Hahn, "Influence of Al particle size and firing profile on void formation in rear local contacts of silicon solar cells," *IEEE Journal of Photovoltaics*, vol. 6, no. 1, pp. 68–73, 2016.

[25] J. C. Zhou, X. Chen, Y. Y. Wang, and B. X. Zhao, "Influence of glass frits on the formation of back surface field in silicon solar cell," *Materials Letters*, vol. 169, pp. 197–199, 2016.

[26] K. S. Choe, "Parametric simulation of the back-surface field effect in the silicon solar cell," *Solid State Sciences*, vol. 29, pp. 48–51, 2014.

[27] J. Krause, R. Woehl, M. Rauer, C. Schmiga, J. Wilde, and D. Biro, "Microstructural and electrical properties of different-sized aluminum-alloyed contacts and their layer system on silicon surfaces," *Solar Energy Materials and Solar Cells*, vol. 95, no. 8, pp. 2151–2160, 2011.

[28] R. Bock, S. Mau, J. Schmidt, and R. Brendel, "Back-junction back-contact n-type silicon solar cells with screen-printed aluminum-alloyed emitter," *Applied Physics Letters*, vol. 96, no. 26, article 263507, 2010.